

# A COMPARATIVE CFD ASSESSMENT STUDY OF CRYOGENIC HYDROGEN AND LIQUID NATURAL GAS DISPERSION

Giannissi, S.G.\* and Venetsanos, A.G.

*Environmental Research Laboratory, National Center for Scientific Research Demokritos, Aghia Paraskevi, Athens, 15341, Greece, [sgiannissi@ipta.demokritos.gr](mailto:sgiannissi@ipta.demokritos.gr), [venets@ipta.demokritos.gr](mailto:venets@ipta.demokritos.gr)*

## ABSTRACT

The introduction of hydrogen to the commercial market as alternative fuel brings up safety concerns. Its storage in liquid or cryo-compressed state to achieve gravimetric efficiency involves additional risks and their study is crucial. This work aims to investigate the behavior of cryogenic hydrogen release and to study the factors that greatly affect vapor dispersion. We focus on the effect of ambient humidity and air's components (nitrogen and oxygen) freezing, in order to identify the conditions under which these factors have considerable influence. The study reveals that humidity reduces conspicuously the longitudinal distance of the Lower Flammability Limit (LFL). Simulations with liquid methane release have been also performed and compared to the liquid hydrogen simulations, in order to detect the differences in the behavior of the two fuels as far as the humidity effect is concerned. It is shown that in methane spills the buoyancy effect in presence of humidity is much smaller than in hydrogen spills and almost negligible.

\*Corresponding author. Tel. +30 210 6503416

Keywords: LH2, LNG, ADREA-HF, dispersion, simulation

## 1 INTRODUCTION

The efficient storage and handling of gaseous fuels, such as hydrogen and natural gas, can be accomplished by their liquefaction at low temperatures. Another recent technology developed for hydrogen automobile applications is the storage under cryo-compressed conditions, i.e. high pressure and low temperature. The accidental release under cryogenic storage conditions involves severe risks and the accompanied potential hazards should be identified.

The physical phenomena associated with cryogenic releases are very complex and have not been studied in depth. One of the main parameters that distinguish cryogenic releases from other releases is the extremely low temperatures that prevail near the release point. At such low temperatures ambient humidity liquefies or even freezes. In case of liquefied hydrogen (LH2) spill or cryo-compressed hydrogen (CCH2) release the temperature is even lower than the freezing point of air components (nitrogen and oxygen) leading to their freezing as well [1]. In case of liquefied natural gas (LNG) spill only humidity phase change takes place.

The phase change of humidity, nitrogen and oxygen leads to two conflicting phenomena: positive buoyancy effect due to heat liberation and increase of mixture density due to formation of non-vapour phase (liquid and solid), which results in dense cloud behavior. The two effects occur simultaneously, but based on [2] the positive buoyancy effect seems to dominate in LNG releases. In [2] is also mentioned that there is little difference to the concentration of methane in the presence of humidity based on experience. However, that statement is not fully validated. All LNG experiments have been performed in open environment with fixed humidity level and no comparison is carried out with counterpart experiments without humidity. The same concerns also the majority of the simulations.

Most LNG and LH2 spill modeling studies neglect humidity and treat air as one component without permitting its freezing. In some LNG simulations, humidity has been taken into account by changing the thermodynamic properties of the air [3]. However, no phase change was considered. In [4] ambient humidity was taken into account in LNG dispersion, however, there was no comparison with the case without humidity. A very recent work [5] examines the effect of modeling the humidity phase change in LNG spills comparing them with experimental data from Burro [6] and Coyote [7] trials and with their counterpart simulations without accounting for humidity phase change. They concluded that the results with modeling the phase change are more consistent with the experimental data by increasing the predicted methane concentration at the presented sensors. However, for Burro trials the humidity effect was small and as time progressed it became negligible.

Giannissi et al. [8] conducted a relevant study in LH2 spills based on experiments performed by Health and Safety Laboratory (HSL) [1] and showed that by taking into account ambient humidity the cloud becomes more buoyant. The air's component liquefaction effect in LH2 spills has been studied in the past by Ichard et al. [9], who performed simulations based on the same HSL experiments modeling test 6 and test 7. Test 6 involves the vertical spill of LH2 100 mm above concrete ground, while test 7 involves horizontal LH2 spill 860 mm above the ground. It was shown that the air's components liquefaction results in more buoyant cloud in test 6, whereas it is reported that it has no effect in test 7. For CCH2 releases is stated in [10] that temperatures are sufficiently low for nitrogen and oxygen to freeze. However, no further analysis has been performed on that subject in the past.

All the above reveal the need of a thorough study, in order to determine the level of influence of the condensation/freezing effect of ambient humidity in LH2, CCH2 and LNG spills and the air's components condensation/freezing effect in both LH2 and CCH2 releases. A reliable tool to perform such analysis is the Computational fluid dynamics (CFD) methodology. Therefore, in the present study the humidity phase change effect on dispersion during LH2 and LNG spill and the nitrogen and oxygen phase change effect on dispersion during LH2 and CCH2 release is studied using the ADREA-HF CFD code. To model the non-vapour phase the Homogeneous Equilibrium Model (HEM) is employed and it is assumed that the non-vapour phase is dispersed in the vapour phase.

For the analysis a series of simulations with different release conditions were conducted with and without humidity imposing several humidity levels. The release conditions were estimated based on characteristic storage conditions for LH2, LNG and CCH2 releases. Simulations that take into account the air's component freezing were also conducted. The predictions were compared with each other and significant conclusions are drawn.

## **2 ACCIDENT SCENARIOS**

For the analysis of the current study several hypothetical accident scenarios are simulated, which correspond to typical release conditions in liquefied hydrogen (LH2), liquefied natural gas (LNG) and cryo-compressed hydrogen (CCH2). For the CCH2 relatively low storage pressures were chosen (up to 55 bar), because very high storage pressure would lead to high jet momentum and there was the intuition that this would result in negligible humidity effect. This was actually verified later by the simulations (Section RESULTS AND DISCUSSION) and thus higher storage conditions were not tested. All simulations involve horizontal cryogenic release 1 m above the ground in stagnant environment. The ambient temperature is 288.15 K. Several release rates, nozzle diameter sizes and humidity levels are examined. For the natural gas simulations only methane is considered. Table 1 summarizes the examined scenarios.

Table 1. Summary of the examined accident scenarios.

Case	Released substance	Storage conditions		Nozzle conditions	Diameter (mm)	Mass flow rate (kg/s <sup>2</sup> )	Froude number	Reynolds number	Relative humidity (RH, %)	Examined effect
		P (bar)	T (K)							
LH2_1	Hydrogen	2	22.9	P=1.01 bar T <sub>sat</sub> = 20.35 K (two-phase, q <sub>v</sub> =6%)	26.6	0.07	16.7	372,283	0	Humidity, air phase change
LH2_2									20	
LH2_3									50	
LH2_4									99	
CCH2_1a	Hydrogen	10	30	P=7.3 bar, T=29.4 K (liquid phase)	1	0.004	1006	634,408	0	Humidity, air phase change
CCH2_2a									20	
CCH2_3a									50	
CCH2_4a									99	
CCH2_1b	Hydrogen	50	48	P=18 bar, T=36.3 K (supercritical)	1	0.0094	4577.52	1,366,865	0	Humidity, air phase change
CCH2_3b									50	
CCH2_4b									99	
CCH2_1c	Hydrogen	50	48	P=18 bar, T=36.29 K (supercritical)	0.1	9.4·10 <sup>-5</sup>	14475.4	136,686.542	0	Humidity phase change
CCH2_4c									99	
CCH2_1d	Hydrogen	55	30	P=4.16 bar, T=26.28 K (liquid phase)	22.5	9.8	849.3	60,543,714.59	0	Humidity phase change
CCH2_4d									99	
LNG_1	Methane	2	120.6	1.01 bar, T=111.5 (two-phase, q <sub>v</sub> =6%)	26.6	0.08	11.4	18,478.1	0	Humidity phase change
LNG_3									50	
LNG_4									99	

The source conditions represent the conditions at the nozzle. In the cryo-compressed releases to calculate the nozzle conditions and to model the under-expanded jet the release modeling and the notional nozzle approach proposed by [11] were used. In the simulations the notional nozzle conditions were set as hydrogen inlet conditions, which are shown in Table 2. The storage conditions

in the CCH2 simulations are chosen randomly, in order specific velocity magnitudes to be obtained at the nozzle for the analysis's purpose.

Table 2. Conditions at notional nozzle for the CCH2 simulations.

	Diameter (mm)	Temperature (K)	Volume fraction (dimensionless)	Velocity (m/s)
Case a	5.2	29.4	1	220.92
Case b	5.45	36.3	1	585.05
Case c	0.545	36.3	1	585.05
Case d	17.65	26.27	1	407.88

In the LH2 simulations the storage conditions and orifice size were chosen equal to the values of the HSL experiments [1] related to LH2 spill. The mass flow rate was calculated by the Fauske and Epstein equation [12] for saturated liquids as suggested also by [13],

$$\dot{m} = \left[ AL / (\rho_v^{-1} - \rho_l^{-1}) \right] (T_s c_{pl})^{-1/2} \quad (1)$$

where  $\dot{m}$ -mass flow rate, kg/s; A-the orifice area, m<sup>2</sup>; L-latent heat of vaporization, J/kg;  $\rho$ -density, kg/m<sup>3</sup>; T-storage temperature, K;  $c_{pl}$ -specific heat of liquid, J/kg/K. The mass flow rate computed by eq. (1) is lower than the measured mass flow rate (0.07kg/s). This was attributed to the frictional losses. Therefore, to account for the frictional losses the computed mass flow rate is multiplied by a factor F as suggested by [12] equal to approximately 0.056.

For the LNG simulations to have comparable release conditions with the LH2 case the same release characteristics (storage conditions, orifice size, frictional factor) were applied. The mass flow rate was found equal to 0.08 kg/s.

In the above calculations for the fluid properties, e.g. density, the NIST equation of state was used, while for the dispersion modeling the ideal gas assumption was made in all simulations. The ideal gas approximation is valid in the dispersion modeling, because pressure is equal to atmospheric. At very low temperatures and ambient pressure the gas behavior deviates from the ideal gas behavior (Figure 1). However, the extremely low temperatures with the largest deviation from ideal behavior are achieved only in a limited area near the spill point. Thus, the non-ideal effects are expected to be small.

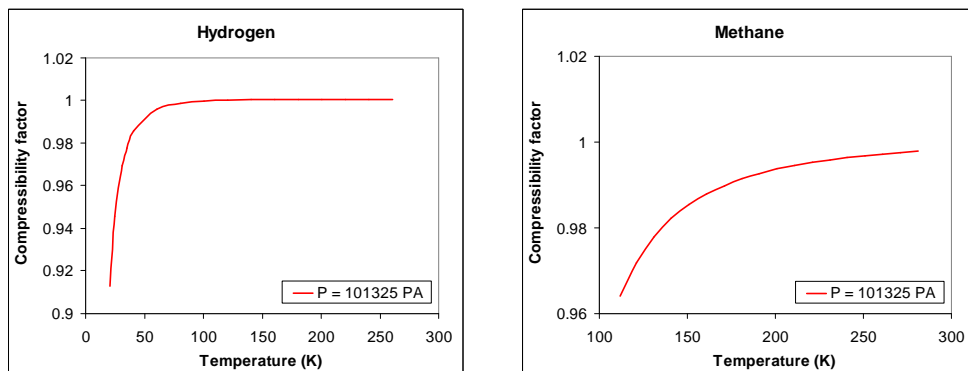


Figure 1. Compressibility factor at atmospheric pressure (based on the NIST equation of state).

The densimetric Froude and Reynolds numbers shown in Table 1 are calculated at the nozzle conditions and their value is derived by,

$$Fr = \frac{u}{\sqrt{g|\rho_{\text{air}} - \rho_p|/\rho_p d}}, \quad Re = \frac{\rho_p u d}{\mu_p} \quad (2)$$

where  $u$  - velocity vector, m/s;  $g$  - gravitational acceleration vector, m/s<sup>2</sup>;  $d$  - diameter, m;  $\mu$  - dynamic viscosity, kg/m.s. Index  $p$  is for the released substance, e.g. hydrogen.

### 3 SIMULATION SETUP

For the simulations the ADREA-HF CFD code is used. ADREA-HF code is a three dimensional time dependent finite volume code that has been validated in several dispersion problems [14], in LH2 [8], LNG [15], and CCH2 releases [11]. For the multiphase modeling the dispersed model is employed, in which the non-vapour phase (liquid and solid) is assumed to be dispersed in the vapour phase. The Homogeneous Equilibrium Model (HEM) is used, according to which all phases are in thermodynamic and hydrodynamic equilibrium, i.e. they share the same pressure and temperature and they have the same velocity. Slip effects between phases are not accounted in the present study to simplify the problem.

#### 3.1 Mathematical equations

The equations that are solved are the mass, momentum and energy conservation equations for the mixture along with the conservation equation of the species mass fraction,

$$\frac{\partial \rho}{\partial t} + \frac{\partial \rho u_i}{\partial x_i} = 0 \quad (3)$$

$$\frac{\partial \rho u_i}{\partial t} + \frac{\partial \rho u_i u_j}{\partial x_j} = -\frac{\partial P}{\partial x_i} + \frac{\partial}{\partial x_j} \left( (\mu + \mu_t) \left( \frac{\partial u_i}{\partial x_j} + \frac{\partial u_j}{\partial x_i} \right) \right) + \rho g_i \quad (4)$$

$$\begin{aligned} \frac{\partial \rho h}{\partial t} + \frac{\partial \rho u_i h}{\partial x_i} &= \frac{dP}{dt} + \frac{\partial}{\partial x_i} \left( (\lambda + \lambda_t) \frac{\partial T}{\partial x_i} \right) \\ &+ \frac{\partial}{\partial x_i} \left( \rho \sum_{k \neq a} D_{qk} (h_{v_k} - h_{v_a}) \frac{\partial q_{v_k}}{\partial x_i} \right) + \frac{\partial}{\partial x_i} \left( \sum_k \frac{\mu_t}{Sc_t} h_k \frac{\partial q_k}{\partial x_i} \right) \end{aligned} \quad (5)$$

$$\frac{\partial \rho q_p}{\partial t} + \frac{\partial \rho u_j q_p}{\partial x_j} = \frac{\partial}{\partial x_j} \left( \left( \rho D_p + \frac{\mu_t}{Sc_t} \right) \frac{\partial q_p}{\partial x_j} \right) \quad (6)$$

where  $\rho$  - mixture density, kg/m<sup>3</sup>;  $P$  - pressure, Pa;  $\mu$ ,  $\mu_t$  - laminar and turbulent viscosity respectively, kg/m.s;  $\lambda$ ,  $\lambda_t$  - laminar and turbulent thermal conductivity respectively,  $Sc_t$  - turbulent Schmidt number, dimensionless;  $d$  - molecular diffusivity, m<sup>2</sup>/s;  $h$  - enthalpy, J/kg;  $q$  - mass fraction. Turbulent Schmidt number is set equal to 0.72. The subscripts  $i, j$  denote the Cartesian  $i$  and  $j$  coordinate, respectively, index  $p$  denotes the component  $p$ , index  $v$  is for the vapour phase and index  $a$  is for air. In eq. (6) the total mass fraction (vapour and non vapour phase) of each mixture component (e.g. hydrogen) is implied.

In the case of hydrogen release the hydrogen mass fraction is solved, while in the LNG simulations the mass fraction of methane is solved. The mass fraction of air is obtained considering that the summation of each component's mass fraction equals unity. When humidity is taken into account the mass fraction of water is solved additionally, while when air is modeled as nitrogen and oxygen, the mass fraction of oxygen is also solved. Nitrogen mass fraction is obtained similarly to air mass fraction as mentioned above. However, phase change is permitted also in nitrogen.

For the turbulence modeling the k- $\epsilon$  model is used with extra source terms for buoyancy [14]. The phase distribution of components is calculated using the Raoult's law for ideal mixture. The solid phase of component-p appears when the mixture enthalpy falls below the enthalpy of solidification of component-p.

For the time integration the first order implicit scheme was used. In the momentum equation the MUSCL high order scheme was employed for discretization of the convective terms.

### 3.2 Computational domain, grid and boundary conditions

In all simulations symmetry along y-axis is assumed. In the LH2 simulations the domain was extended 1 m upwind the nozzle and 15 m downwind the nozzle along x-direction and 5 m along the y-direction. The boundary in the z-direction was set at 40 m height. Refinement was imposed close to the spill point with minimum cell size equal to the nozzle diameter. Expansion ratios from 1.05 close to the nozzle to 1.12 further downwind were applied. The total number of cells was 253,800.

In the LNG simulations the domain was larger than the LH2 simulations. In the x-direction the domain was extended 40 m downwind the release point. Along y-direction the domain was extend 50 m, while the height of the domain is 5 m. The rest grid characteristics were the same as in the LH2 simulations. The total number of cells was 277,032.

In the CCH2 simulations with the smaller release rate (case c:  $9.4 \cdot 10^{-5}$  kg/s) the domain was extended 12 mm and 2 m upwind and downwind the nozzle, respectively, along x-direction. Along y-direction it was extended 0.25 m and the domain size in z-direction was 0.4 m (0.2 m above and below the nozzle). In simulations of case a (0.004 kg/s) a larger domain was used with extension along x-direction 12 mm and 7 m upwind and downwind the nozzle, respectively,. Along y-direction the domain was extended 0.5 m and its size in z-direction was set equal to 3 m. In the simulations of case b (0.009 kg/s) a smaller domain was designed in z-direction (2 m) and a larger domain in x-direction (12 m downwind the nozzle). Finally, in the simulations with the largest release rate (case d: 9.8 kg/s) the domain was extended 15 m upwind the nozzle and 200 m downwind the nozzle. Along y-direction it was extended 10 m and in z-domain size was 100 m. In all cases refinement was imposed near the nozzle with minimum cell size equal to the nozzle diameter and expansion ratios 1.05-1.12. The total number of cells was 196 560, 182 160, 445 060 and 127 650 for cases a, b, c and d, respectively.

In all simulations the hydrogen inlet was modelled as a source area on the face of the control volume located exactly at the release point. Only one cell was used to discretize the source. Since the grid that was used is Cartesian, a squared-shape source area was used with the same area as the circular source area (notional source area in the CCH2 simulations), in order to be fully aligned with the grid.

A transient one-dimensional heat transfer equation was solved inside the underground to obtain the interface temperature on the bottom boundary in the simulations. In all open boundaries a constant pressure condition was applied, except for the downwind outlet boundary where zero gradient was imposed considering that the domain was sufficiently extended.

## 4 RESULTS AND DISCUSSION

Figure 2 and Figure 3 show the steady state concentration contours on symmetry plane for the LH2 and LNG simulations, respectively, with and without modeling humidity. It is shown that in LH2 simulation the humidity effect is significant and the higher the relative humidity (RH) is the higher the effect close to the spill point. The cloud becomes more buoyant resulting in reduction of the longitudinal distance of the flammable cloud by approximately 27% for RH 99%. The induced buoyancy is attributed to the heat liberation by the phase change of water [8]. From safety point of view this feature is significant and thus ambient humidity reduces the associated risks in case of an accidental hydrogen spill. However, it seems also that the volume of premixed hydrogen-air within the detonability limits (18.3-59% v/v) is increased near the spill point in presence of humidity.

For RH 20% the humidity effect seems small and the Lower Flammability Limit (LFL) horizontal distance is not influenced greatly. As LFL 4% v/v and 5% v/v concentration is assumed for hydrogen and methane, respectively. One should keep in mind that for different ambient temperature the same relative humidity corresponds to different specific humidity (fraction of water mass to total moist air mass). The specific humidity is actually the significant parameter. Test simulations with higher ambient temperature showed that the humidity effect is more enhanced due to the higher water mass fraction, e.g. simulations with ambient temperature 298.15 K and RH 50% reduce the LFL distance by about 35 %.

The cloud without humidity or low humidity level seems to reach higher heights, probably due to the higher heat conducted by the ground in the examined case. In the simulation with RH 99% the flammable cloud is lifted near the spill point and comes in less contact with the ground.

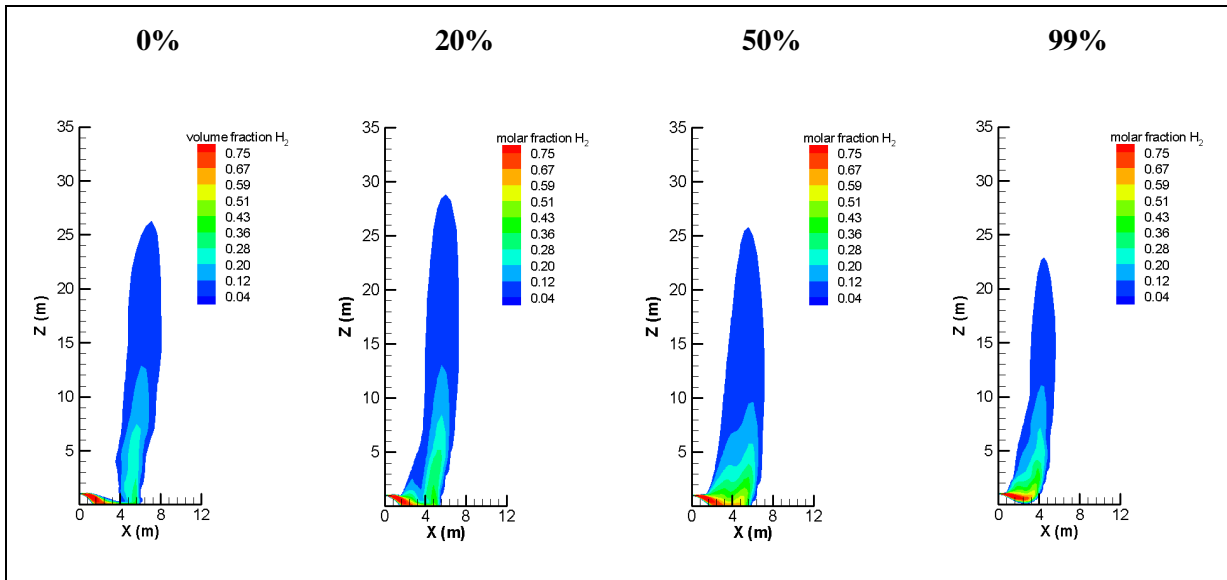


Figure 2. Humidity effect: Steady state  $H_2$  concentration contours (within flammable range) on symmetry plane for the LH2.

In LNG simulations the buoyancy effect is not pronounced. The methane concentration within the flammable limits seems not to be greatly influenced by the humidity condensation/freezing even for almost saturated air (RH 99%). This notable discrepancy from hydrogen behavior in presence of humidity might be happening because methane becomes lighter than air for temperatures higher than 160 K at ambient pressure. Thus, even if temperature is increased the cloud still has dense to passive behavior, as mentioned also in [2]. Temperatures higher than 160 K correspond mainly to lower than the LFL concentrations. Within the flammable range there is only a very limited area near the ground and 2 m downwind the release, where the cloud reaches temperatures higher than 160 K, as Figure 3 shows. The longitudinal distance of the flammable cloud seems to be increased (by about 45%) in the

presence of humidity, probably because the mixture density is increased due to the condensed/freezeed water resulting in a heavier than surrounding air cloud.

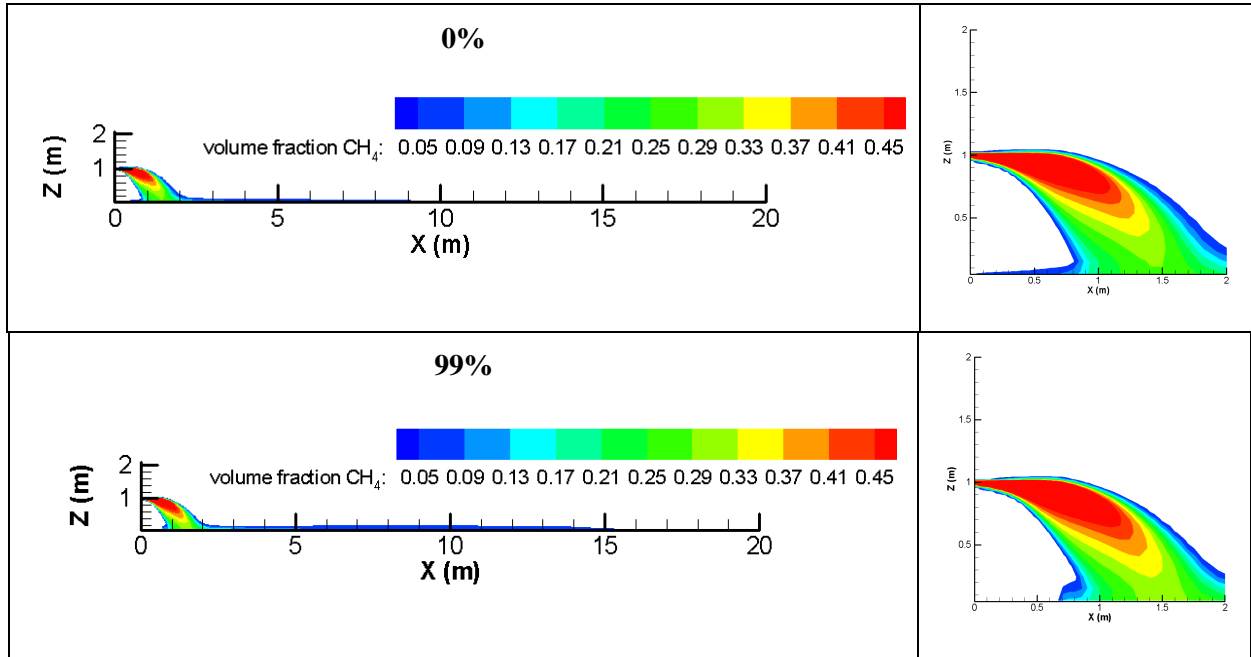


Figure 3. Humidity effect: Steady state  $\text{CH}_4$  concentration (within flammable range) on symmetry plane for the LNG. In the right column a close view near the release is illustrated.

Figure 4 illustrates the flux Richardson number ( $\text{Ri}_f$ ) contours and the temperature contour lines.  $\text{Ri}_f$  is the ratio of buoyant production term to mechanical production term and characterizes the thermal stability of the flow. As shown in the figure,  $\text{Ri}_f$  is positive and above 1 in the area with concentration levels outside of the flammable range, where it is of low importance for safety assessments. In that area the cloud can be regarded as buoyant.

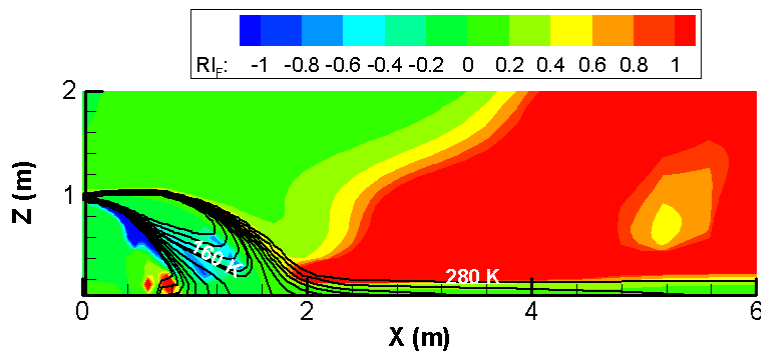


Figure 4. Temperature contours lines and flux Richardson number contour flood for the LNG case with 99% relative humidity.

Figure 5 and Figure 6 show the hydrogen concentration contours on symmetry plane for the CCH2 simulations. It is shown that humidity effect is significant only for the simulations with low  $\text{Fr}$  (case a and d) at the nozzle (Table 1) and relatively high RH. Simulation of case a with RH 20% did not have any significant impact on cloud buoyancy; hence it is not shown here. Similar to the LH2 case the specific humidity is the most significant factor, thus high specific humidity is necessary for the cloud to become buoyant. The horizontal LFL distance is reduced by about 25% and 30% for case a and d,



respectively, when humidity (RH=99%) is modelled. In case d (low Fr but high Re) the buoyancy effect is apparent only further downwind the release, where the momentum dominant region is weakened. Near the release despite the low Fr number (=849), humidity seems not to affect the cloud due to the high jet momentum. For that phenomenon to occur the release conditions should be such that the flammable cloud would travel further downwind, e.g. high release rate. In releases with high Fr number (case b and c) the jet near the release point, where temperatures are low enough for the humidity to freeze, lies at momentum dominant region and thus the buoyancy effect is small even for case c which has low Re number. Therefore, it can be concluded that the factor that determines if the humidity effect would be significant is mainly the Fr number at the nozzle. Re number is an indicator of whether the effect would be significant near the nozzle (if it is low) or only at a distance from the nozzle (if it is high).

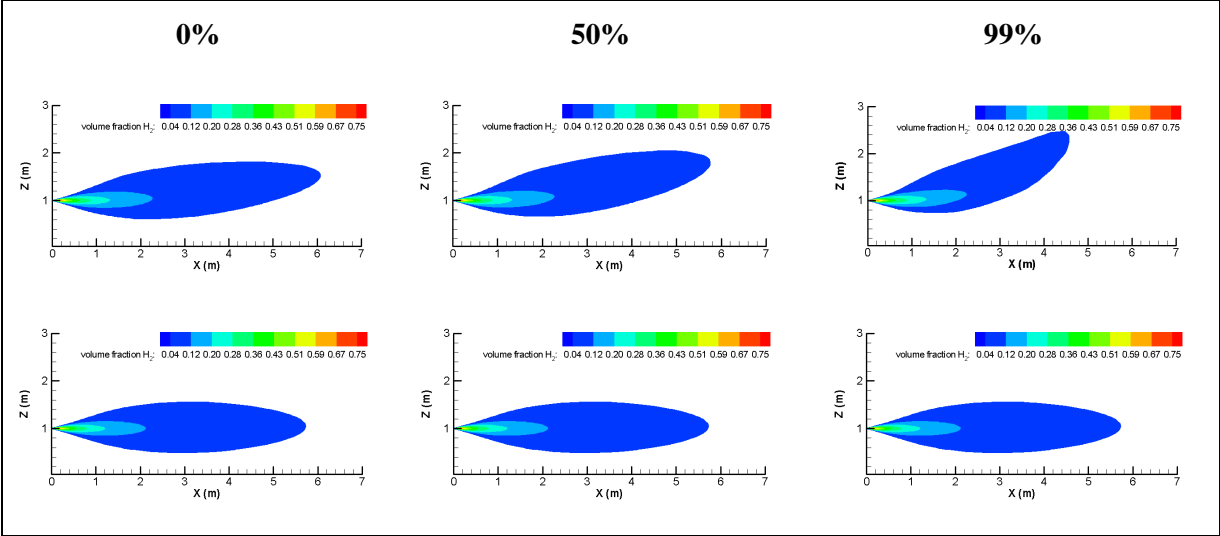
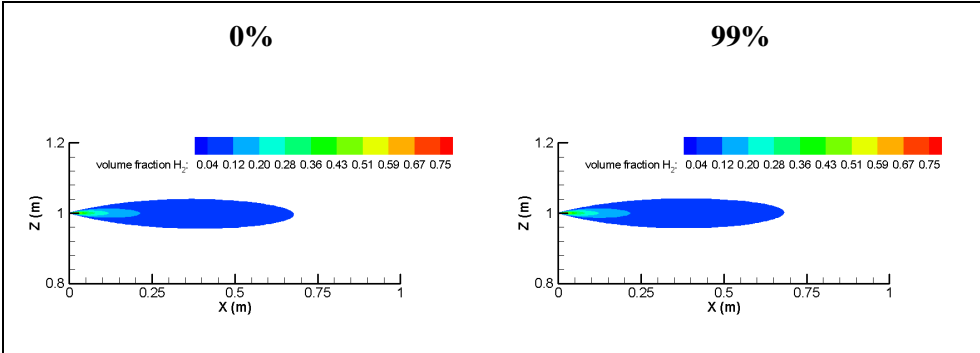


Figure 5. Humidity effect: Steady state H<sub>2</sub> concentration (within flammable range) on symmetry plane for the CCH<sub>2</sub>, top: case a, bottom: case b.

Based on Table 1 the accident scenarios with low Fr number at the nozzle correspond to liquid flow at the nozzle and in liquid storage conditions. Considering also the fact that in the LH<sub>2</sub> spill scenario two-phase flow with low vapour mass fraction occurs at the nozzle, then it is most likely that humidity effect would be significant in CCH<sub>2</sub> releases if liquid or two-phase (with low vapour mass fraction) flow occurs at the nozzle. Such conditions can be achieved during the isentropic expansion from stagnation to nozzle conditions [11] if hydrogen is stored in liquid state or in supercritical state in the side of the saturated liquid line (left side on the temperature-entropy chart).



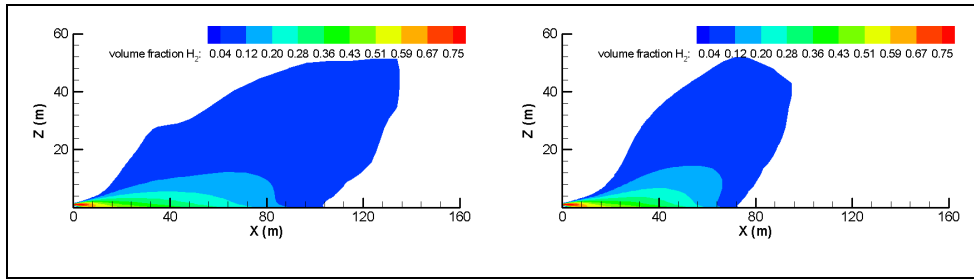


Figure 6. Humidity effect:  $H_2$  concentration (within flammable range) on symmetry plane for the CCH2, top: case c, bottom: case d.

Figure 7 and Figure 8 show the flammable cloud at steady state on symmetry plane for the LH2 and the CCH2 simulations (case a), respectively with and without modeling the air's component phase change (humidity is not modeled).

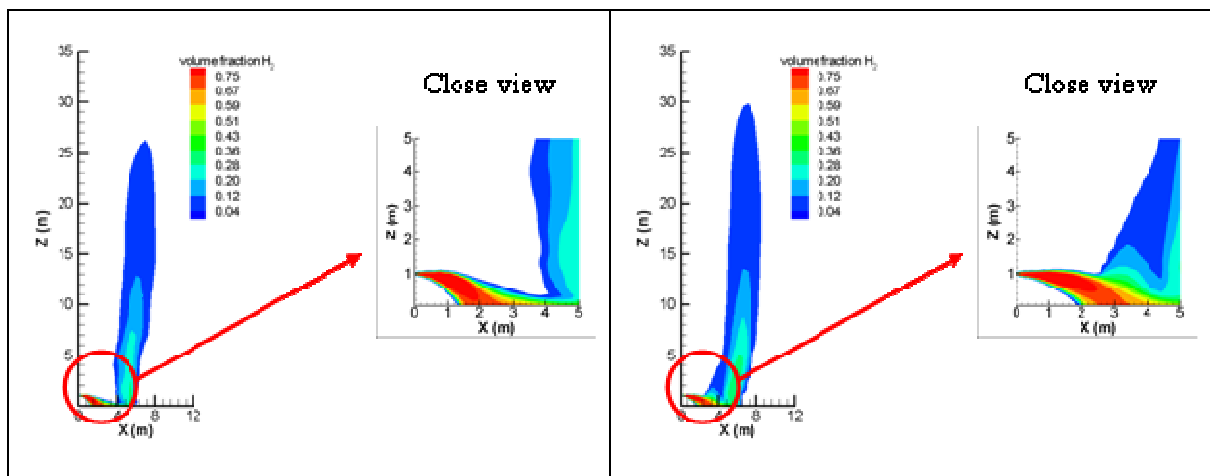


Figure 7. Steady state  $H_2$  concentration contours on symmetry plane for the LH2 without air's component phase change (left) and with air's component phase change (right).

It is shown that in the LH2 simulation there is an effect of air's component freezing on mixture dispersion. The cloud is lifted more and the induced buoyancy is evident near the spill point, where the phase change occurs, as shown in Figure 7 (in the close view image). Buoyancy is produced by the heat liberation of  $N_2$  and  $O_2$  phase change. In the CCH2 simulations (case a and b) the effect is negligible, because the  $N_2$  and  $O_2$  freezing occurs in a very limited area near the nozzle where the momentum forces are the dominant forces. Here the concentration contours only for case a are shown for space economy. Similar behavior is observed for case b too.

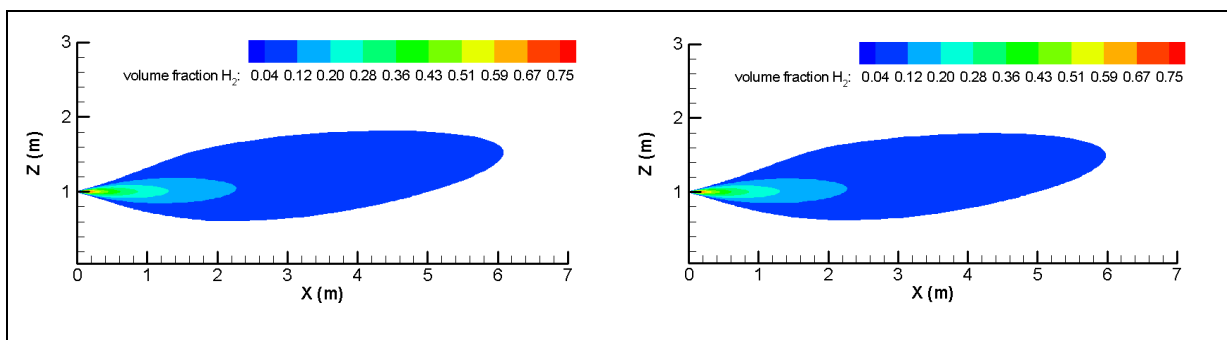


Figure 8. Steady state  $H_2$  concentration contours on symmetry plane for the CCH2 (case a) without air's component phase change (left) and with air's component phase change (right).

## 5 CONCLUSIONS

A Computational Fluid Dynamics (CFD) study of the humidity effect on liquid hydrogen (LH2), cryo-compressed hydrogen (CCH2) and liquid natural gas (LNG) dispersion in stagnant environment is carried out and its level of influence is discussed. Characteristic storage conditions were applied in all cases, in order to estimate the release conditions. In hydrogen releases, both liquid and cryo-compressed, the effect of air components' freezing is also examined. The entire analysis is performed using the CFD code, ADREA-HF.

According to the analysis in LH2 spills the condensation/freezing of humidity makes the cloud more buoyant and in the presence of humidity the longitudinal Lower Flammability Limit (LFL) distance is significantly reduced (approximately 27% for ambient temperature equal to 288.15 and relative humidity 99%). The higher the water mass fraction (i.e. specific humidity) is in air the higher the effect would be and thus in warmer environments for the same relative humidity percentage the effect is expected to be higher. In LNG spills humidity exhibits only a modest influence on the buoyancy of the mixture. This may be attributed to the fact that methane stops behaving as dense gas above 160 K at ambient pressure and higher than 160 K temperatures are developed mainly in a region with concentration levels lower than the LFL. This behavior is also verified by the flux Richardson number, which is below or equal to unity in the largest part of the domain with considerable methane concentration, meaning that the flammable cloud can be regarded as dense or passive.

In the cryo-compressed releases the humidity effect depends on the jet momentum, which can be interpreted in terms of Fr and Re number at the nozzle. For the case with  $Fr \approx 10^3$  and  $Re \approx 6.3 \cdot 10^5$  the humidity effect on dispersion was apparent. The cloud became more buoyant at a distance from the nozzle, where the jet entered the buoyant region and the momentum forces were less enhanced. For the case with  $Fr \approx 4.5 \cdot 10^3$  and  $Re \approx 1.3 \cdot 10^6$  the effect was negligible. For the case with very high Fr number ( $\approx 1.4 \cdot 10^4$ ) but low Re number ( $\approx 1.4 \cdot 10^5$ ) the humidity effect was insignificant, while for the case with low Fr number ( $\approx 849$ ) and high Re number ( $\approx 6.0 \cdot 10^7$ ) the effect was apparent mostly further downwind the release. Based on these remarks it can be concluded that Fr number is the parameter that mainly indicates whether the humidity effect would be significant. For low Fr number (below  $10^3$ ) the humidity effect cannot be neglected. Re number assist the flow characterization but it was shown that high Re does not necessarily means that the humidity effect would be negligible in the entire domain. In the future more detailed analysis can be conducted, in order to find a critical value for Fr number for the humidity effect to be significant.

Considering all the above, it can be concluded that in liquefied hydrogen releases at low storage pressure the humidity effect is significant and should be always taken into account in simulations, because low Fr is achieved at the spill point. This is attributed to the low spill velocities that are developed at the orifice due to the high liquid density. On the contrary, in CCH2 releases humidity effect can be significant and should be modeled only for low Fr number at the nozzle. Such conditions can be achieved most likely if stagnation conditions correspond to liquid state or supercritical state in the side of the saturated liquid line, in order liquid flow or two-phase flow with low vapour quality to occur at the nozzle during the isentropic expansion. Moreover, in cryo-compressed releases stored at extremely high pressure (e.g. 200 bar) the momentum forces would be the most dominant and thus the humidity effect is expected to be diminished and almost negligible.

As far as the air's component phase change is concerned, its effect is perceptible in LH2 spills, while it is negligible in CCH2 releases due to the fact that it occurs only at a small region close to the nozzle where jet momentum dominates. Thus, in LH2 simulations the air's component phase change is recommended to be taken into account, while in CCH2 simulations it can be neglected without losing accuracy in concentration predictions.

## ACKNOWLEDGEMENTS

The first author gratefully acknowledges the financial support received from “IKY FELLOWSHIPS OF EXCELLENCE FOR POSTGRADUATE STUDIES IN GREECE – SIEMENS PROGRAM”. The authors would also like to thank the SUSANA project, which has received funding from the European Union's Seventh Framework Programme (FP7/2007-2013) for the Fuel Cells and Hydrogen Joint Technology Initiative under grant agreement n° FCH-JU-325386.

## REFERENCES

1. Hooker, P., Willoughby, D.B. and Royle, M., Experimental releases of liquid hydrogen, 4th Int. Conf. on Hydrogen Safety, San Francisco, CA, USA, paper 160, 2011.
2. Ivings, M., Jagger, S. and Lee, C., Evaluating vapor dispersion models for safety analysis of LNG facilities research project, Fire Prot. Res. Found., April 2007.
3. Cormier, B.R., Qi, R., Yun, G., Zhang, Y. and Mannan, M.S., Application of computational fluid dynamics for LNG vapor dispersion modeling : A study of key parameters, *J. Loss Prev. Process Ind.*, **22**, No. 3, 2009, pp. 332–352.
4. Giannissi, S.G., Venetsanos, A.G. and Markatos, N., CFD Modeling of LNG Spill: Humidity Effect on Vapor Dispersion, *J. Phys. Conf. Ser.*, **633**, 2015, pp. 12136-12142.
5. Zhang, X., Li, J., Zhu, J. and Qiu, L., Computational fluid dynamics study on liquefied natural gas dispersion with phase change of water, *Int. J. Heat Mass Transf.*, **91**, 2015, pp. 347–354.
6. Koopman, R.P., Baker, J., Cederwall, R.T., Goldwire, H.C. Jr., Hogan, W.J., Kamppinen, L.M., Kiefer, R.D., McClure, J.W., McRae, T.G., Morgan, D.L., Morris, L.K., Spann, M.W. Jr. and Lind, C.D., Burro series data report, LLNL/NWC Rep. No.UCID-19075, V.1-2, Lawrence Livermore Natl. Lab. Berkeley, CA, 1982.
7. Goldwire, H., Rodean, H. and Cederwall, R., Coyote series data report, LLNL/NWC, UCID-19953, Vol.1, 2, 1983.
8. Giannissi, S.G., Venetsanos, A.G., Markatos, N. and Bartzis, J.G., CFD modeling of hydrogen dispersion under cryogenic release conditions, *Int. J. Hydrogen Energy*, **39**, No. 28, 2014, pp. 15851–15863.
9. Ichard, M., Hansen, O.R., Middha, P. and Willoughby, D., CFD computations of liquid hydrogen releases, *Int. J. Hydrogen Energy*, **37**, No. 22, 2012, pp. 17380–17389.
10. Friedrich, A., Breitung, W., Stern, G., Vesper, A., Kuznetsov, M., Fast, G., Oechsler, B., Kotchourko, N., Jordan, T., Travis, J.R., Xiao, J., Schwall, M. and Rottenecker, M., Ignition and heat radiation of cryogenic hydrogen jets, *Int. J. Hydrogen Energy*, **37**, No. 22, 2012, pp. 17589–17598.
11. Venetsanos, A.G. and Giannissi, S.G., Release and dispersion modeling of cryogenic under-expanded hydrogen jets, *Int. J. Hydrogen Energy*, vol. 42 (11), pp. 7672-7682, 2017.
12. Fauske, H.K. and Epstein, M., Source term considerations in connection with chemical accidents and vapor cloud modeling, Int. Conf. on Vapor Cloud Modeling, CCPS/AIChE, 345 E. 47th St., New York, NY 10017, pp. 251–273, 1987.
13. Hanna, S.R. and Strimaitis, D., Workbook of test cases for Vapor Cloud Source Dispersion Models. 1989, p. 122.
14. Venetsanos, A.G., Papanikolaou, E. and Bartzis, J.G., The ADREA-HF CFD code for consequence assessment of hydrogen applications, *Int. J. Hydrogen Energy*, **35**, No. 8, 2010, pp. 3908–3918.
15. Giannissi, S.G., Venetsanos, A.G., Markatos, N. and Bartzis, J.G., Numerical simulation of LNG dispersion under two-phase release conditions, *J. Loss Prev. Process Ind.*, **26**, No. 1, 2013, pp. 245–254.